

Explicit Finite Element Models of Friction Dampers in Forced Response Analysis of Bladed Disks

E. P. Petrov

Centre of Vibration Engineering,
Mechanical Engineering Department,
Imperial College London,
South Kensington Campus,
London SW7 2AZ, UK
e-mail: y.petrov@imperial.ac.uk

A generic method for analysis of nonlinear forced response for bladed disks with friction dampers of different designs has been developed. The method uses explicit finite element modeling of dampers, which allows accurate description of flexibility and, for the first time, dynamic properties of dampers of different designs in multiharmonic analysis of bladed disks. Large-scale finite element damper and bladed disk models containing 10^4 – 10^6 degrees of freedom can be used. These models, together with detailed description of contact interactions over contact interface areas, allow for any level of refinement required for modeling of elastic damper bodies and for modeling of friction contact interactions. Numerical studies of realistic bladed disks have been performed with three different types of underplatform dampers: (i) a “cottage-roof” (also called “wedge”) damper, (ii) seal wire damper, and (iii) a strip damper. Effects of contact interface parameters and excitation levels on damping properties of the dampers and forced response are extensively explored. [DOI: 10.1115/1.2772633]

Introduction

Due to the high modal density of natural frequencies of realistic bladed disks and of a broad spectrum of aerodynamic excitation forces, complete prevention of the occurrence of resonance regimes is not feasible. Hence, special devices that dissipate energy of vibrations and reduce resonance amplitudes to acceptable levels are commonly used in practical bladed disks. One of the most effective types of damping devices is a friction damper. This is generally a small piece of metal that can be fitted under platforms or shrouds of adjacent blades. When relative motion of adjacent blades becomes large enough, and micro- or, in some cases, even macroslip starts at damper contacting surfaces, the rubbing dissipates vibrational energy. Moreover, dampers stiffen a structure, which can significantly affect resonance frequencies of a bladed disk. The total damper stiffening effect depends on the stiffness of the damper body and the stiffness of the blade-damper friction contact interfaces. The stiffness properties of damper contact interfaces are dependent on the relative motion of pairing contact surfaces, and the dynamic stiffness of the damper body varies with vibration frequency, which can have significant effect, especially for highly flexible dampers.

There is more than 30 years of history of development of models for dynamic analysis of bladed disks with friction dampers. Yet, underplatform damper (UPD) models have been developed to date only for dampers of simple geometric shape (for the so-called wedge or cottage-roof dampers). In real conditions, such underplatform friction dampers have two interfaces at which they interact with adjacent blades. In order to allow for prediction of the forced response in conjunction with multi-degree-of-freedom (multi-DOF) blade models, several “kinematic” models for cottage-roof dampers have been developed, e.g., in Refs. [1–5]. These models are based on some kinematic hypotheses about the relative motion of a wedge-shaped damper and blade platform,

and, hence, the damper’s dynamics is ignored and inertia forces are neglected. As a result, the friction forces are expressed, in these models, through motion of the blade platforms. In order to describe microslip at the contact interfaces, two approaches were explored: (i) representation of friction contact by an array of spring-slider elements with different parameters (see Ref. [1]) and (ii) use of an analytical solution for friction forces between a bar and a foundation supporting this bar (see Refs. [2,3]). Characterization of such UPD models and analysis of the effects of damper contact stiffness are performed in Refs. [6–8]. Assessment of dampers’ dissipation and stiffness effects, in reducing the forced response, is made in Ref. [9]. UPDs of semicylindrical and wedge shapes were studied in Ref. [10] with allowance for damper stiffness and inertia forces due to rigid-body motion.

Dynamic UPD models, in conjunction with multiharmonic balance method, have recently been developed for cottage-roof and for two-piece “split” dampers (see Ref. [11]). The first attempt to use the friction contact modeling capabilities and multiharmonic analysis code developed in Ref. [12] was made in Ref. [13] to explore possibilities of forced response analysis of a flexible finite element (FE) damper using a two-blade system. A system composed of two blades and a flexible model of a cottage-roof damper have been analyzed in Ref. [14] using simplified, monoharmonic representation for nonlinear forced response.

However, simplifying assumptions introduced in existing damper models, such as the neglect of damper inertia or other dynamic properties, including the damper’s vibration modes, and neglect of inhomogeneity of stress distribution over contact interfaces and contact-separation transitions, significantly restrict the accuracy and area of applicability of these models.

Moreover, there is a tendency to introduce new damper designs in gas-turbine industry. Dampers, such as seal wires or shell-like dampers with very thin walls (see, e.g., Ref. [15]), are very flexible. Their own natural frequencies can be close to and even lower than the natural frequencies of blades. Adequate modeling cannot, therefore, be done without allowing for flexible vibrational modes of dampers and, neither existing kinematic damper models nor even damper models including damper inertia and elasticity, but allowing only rigid-body motion, cannot be used for such highly flexible dampers.

Contributed by the International Gas Turbine Institute of ASME for publication in the JOURNAL OF ENGINEERING FOR GAS TURBINES AND POWER. Manuscript received April 27, 2007; final manuscript received May 24, 2007; published online February 25, 2008. Review conducted by Dilip R. Ballal. Paper presented at the ASME Turbo Expo 2007: Land, Sea and Air (GT2007), Montreal, Quebec, Canada, May 14–17, 2007. Paper No. GT2007-27980.

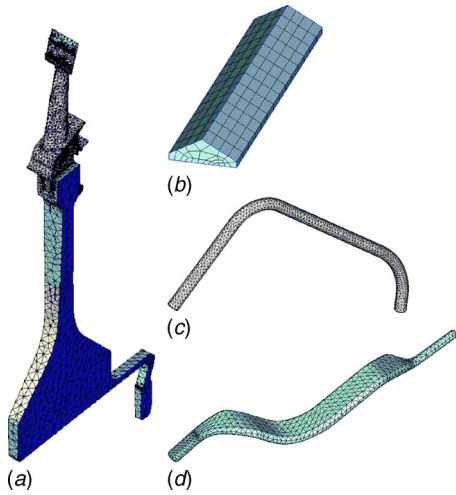


Fig. 1 FE models of (a) a bladed disk sector, (b) a cottage-roof damper, (c) a seal wire damper, and (d) a seal strip damper

Thus, predictive numerical studies could not be performed with acceptable accuracy for bladed disks with many existing and forthcoming types of friction damper design.

In this paper, a generic method for modeling underplatform and other types of friction damper has been developed. The method is based on explicit modeling of friction dampers in the analysis of nonlinear forced response of bladed disks using large-scale FE models. Such high-fidelity models allow accurate description of realistic geometric shapes and dynamic properties of all components of bladed disks, including dampers. As a result, any damper design and geometry can be analyzed, and, moreover, dynamic properties of the friction dampers and blade-damper contact interactions are accurately described without any simplified assumptions, which have been unavoidable hitherto.

Numerical investigations of bladed disks with flexible dampers of different designs are performed to demonstrate and validate the capabilities of the new models. Realistic large-scale FE models of bladed disks and friction dampers containing hundreds of thousands of DOFs are used in the calculations. An analysis of the influence of damper parameters on the forced response of bladed disks is included.

Method for Forced Response Analysis of Bladed Disks With Explicit Damper Models

Modeling of Dampers of Different Design and Bladed Disks. Large-scale FE models are used for the analysis of bladed disks and dampers. The models can frequently comprise millions of DOFs for bladed disks and tens or hundreds of thousands of DOFs for a damper elastic body. Examples of FE models for a bladed disk sector and for dampers of different design are shown in Fig. 1.

For the case of a tuned assembly, a single sector model is used for forced response calculations. A method for the analysis of nonlinear dynamics of structures with cyclic symmetry previously reported in Ref. [16] is used for this case. It allows significant reduction of computational expense while ensuring completeness and accuracy of calculation even for highly nonlinear structures. A method developed in Refs. [17,18] can be applied to a mistuned structure.

Dynamic models of a bladed disk and of a damper can be created separately when dampers are manufactured separately from a bladed disk and are not elastically connected to it. Models of dampers and bladed disks, considered in this section, describe the dynamic properties of elastic bodies of dampers and bladed disks. Because of this, the models are linear, which facilitates determination of their modal characteristics and allows accurate

condensation of the models. Nonlinear friction contact and unilateral contact interaction between damper elastic bodies and blades are taken into account at a later stage, described in this paper in the following section.

For a case of steady-state vibrations, equations of motion for a bladed disk and for a damper can be written in the following form:

$$[(\mathbf{K}_e^{B,D} + \mathbf{K}_g^{B,D} - \Omega^2 \mathbf{M}_\Omega^{B,D}) + i\omega \mathbf{C}^{B,D} - \omega^2 \mathbf{M}^{B,D}] \hat{\mathbf{Q}}^{B,D} = \hat{\mathbf{P}}^{B,D} \quad (1)$$

where $\mathbf{K}_e^{B,D}$ is the conventional elastic stiffness matrix of a bladed disk (superscript B) or of a damper (superscript D), $\mathbf{K}_g^{B,D}(\Omega)$ is the so-called geometric stiffness matrix reflecting the stiffening effects of the centrifugal forces, $\mathbf{M}_\Omega^{B,D}$ is the spin-softening matrix describing the stiffness softening due to the changing direction of the centrifugal forces under vibration; $\mathbf{C}^{B,D}$ and $\mathbf{M}^{B,D}$ are damping and mass matrices, respectively, $i = \sqrt{-1}$, and Ω and ω are the rotation speed and an excitation frequency, respectively. $\hat{\mathbf{Q}}^{B,D}$ is the vector of complex amplitudes of displacements for all DOFs in a FE model of a bladed disk or a damper, and $\hat{\mathbf{P}}^{B,D}$ is the vector of complex amplitudes of excitation forces.

For a tuned bladed disk a single sector can be used for the exact calculation of both free vibration and forced responses of a whole structure. This is achieved by imposing special cyclic symmetry conditions, which describe the interaction of a sector with other sectors of a bladed disk. The cyclic symmetry conditions establish a relationship between DOFs located on the left and right boundaries of a sector, i.e.,

$$\hat{\mathbf{Q}}_{\text{left}}^B = e^{i(2\pi/N_B)m} \hat{\mathbf{Q}}_{\text{right}}^B \quad (2)$$

where N_B is the total number of sectors in a bladed disk and m is the number of deformation waves considered.

In order to allow efficient calculation of nonlinear forced response for bladed disks with dampers interacting at friction contact interfaces, the models provided by Eq. (1) are condensed. The DOFs at the nodes where there are no contact are excluded from the equations; full accuracy of modeling is preserved and forced response for excluded DOFs can still be determined.

The condensation process results in the (i) dynamic compliance, frequency response function (FRF) matrices for DOFs, where contact interactions are expected to occur, and (ii) complex amplitudes of displacements, which are evoked by the excitation forces at the contact nodes.

FRF matrices for a tuned bladed disk without dampers, $\mathbf{A}_m^B(m_j\omega)$, and for the damper(s) are generated from natural frequencies, mode shapes, and modal damping factors:

$$\mathbf{A}_m^B(\omega) = \sum_{r=1}^{N_m^B} \frac{\phi_{rm}^B(\Omega) [\phi_{rm}^B(\Omega)]^*}{[1 - i\eta_{rm}^B(\Omega)][\omega_{rm}^B(\Omega)]^2 - \omega^2} \quad (3)$$

$$\mathbf{A}^D(\omega) = \sum_{r=1}^{N^D} \frac{\phi_r^D(\Omega) [\phi_r^D(\Omega)]^T}{[1 - i\eta_r^D(\Omega)][\omega_r^D(\Omega)]^2 - \omega^2} \quad (4)$$

where $j = \overline{1, n}$, and $\omega_{rm}^B(\Omega)$, $\phi_{rm}^B(\Omega)$, and $\eta_{rm}^B(\Omega)$ are the r th natural frequency, mode shape, and modal damping factor, respectively, for a bladed disk without dampers corresponding to a family of modes with m nodal diameters. $\omega_r^D(\omega)$, $\phi_r^D(\omega)$, and $\eta_r^D(\omega)$ are the r th natural frequency, mode shape, and modal damping factor, respectively, for an individual damper. N_m^B and N^D are the numbers of modes used for the generation of FRF matrices of a bladed disk and a damper, respectively. Superscript $*$ indicates a Hermitian conjugate and superscript T indicates transposition here.

Vectors of mode shapes $\phi_{rm}^B(\omega)$ and $\phi_r^D(\omega)$ contain modal displacements only for nonlinear DOFs. Their components are simply selected from mass-normalized vectors $\hat{\phi}_{rm}^B(\Omega)$ and $\hat{\phi}_r^D(\Omega)$ obtained from the solution of eigenproblem resulting from Eq. (1)

by omitting terms $i\omega\mathbf{C}^{B,D}$ and $\hat{\mathbf{P}}^{B,D}$.

Dependency of all modal characteristics on the rotation speed Ω is allowed here in order to describe the effects of the rotation speed on the modal properties. Modal characteristics are determined for a number of traveling deformation waves m considered in Eq. (1). Mode shapes are calculated using a sector model for a tuned system, and these mode shapes take complex values for all nodal diameter numbers different from 0 and $N_B/2$.

Complex amplitudes of displacements caused by excitation forces distributed over the blade and damper nodes can be very efficiently calculated at the contact nodes as proposed in Ref. [16]:

$$\text{lin}\mathbf{Q}_m^B(\omega) = \sum_{r=1}^{N_B} \frac{[\hat{\phi}_{rm}^B(\Omega)]^* \hat{\mathbf{P}}^B}{[1 - i\eta_{rm}^B(\Omega)][\omega_{rm}(\Omega)]^2 - \omega^2} \phi_{rm}^B \quad (5)$$

$$\text{lin}\mathbf{Q}^D(\omega) = \sum_{r=1}^{N_D} \frac{[\hat{\phi}_r^D(\Omega)]^T \hat{\mathbf{P}}^D}{[1 - i\eta_r^D(\Omega)][\omega_r(\Omega)]^2 - \omega^2} \phi_r^D \quad (6)$$

Multiplication of large vectors, $(\hat{\phi}_{rm}^B)^* \hat{\mathbf{P}}^B$ and $(\hat{\phi}_r^D)^T \hat{\mathbf{P}}^D$, involving all sector DOFs provides a single coefficient for each mode shape, which is usually called "a modal force." These modal forces take into account arbitrary distribution of the excitation forces over all nodes of the bladed disk sector model and of the damper.

Modeling of Blade-Damper Friction Contact Interaction.

The forces acting at friction contact interfaces are generally strongly nonlinear. The nonlinearity of the interaction is due to (i) unilateral contact of interaction along directions normal to contact surfaces, when compression normal stresses can be acted at these surfaces but tension stresses are not allowed; (ii) variation of contact areas during the vibration period, including closing and opening clearances and interferences, and contact-separation transitions over a whole interface surface or some parts of t ; (iii) friction forces whose magnitude and stick-slip transitions are affected by contact separation and normal stress variation.

The friction contact interface models and friction contact elements developed in papers Refs. [19,20] take into account all the above phenomena and allow analytic calculation of interaction force vectors and stiffness matrices for the case of multiharmonic vibration, accurately and very fast. These elements allow modeling of friction contact interactions, which can be localized at a point or distributed over a line or an area. It should be noted that the actual contact conditions experienced by each contact node (e.g., slip, stick, separation, and full contact) are determined as a result of calculation and, therefore, there is no requirement to know nonlinear DOFs a priori. A reasonable guess about DOFs where nonlinear interactions appear simply helps us to reduce the number of DOFs kept in the nonlinear equations. Moreover, actual contact area, which can vary during a vibration period, and energy dissipated by each area friction contact element during the vibration period are also calculated.

Examples of applications of area and line friction contact element are shown in Fig. 2. For a cottage-roof damper (Fig. 2(a)), area contact elements are spread over both contact surfaces of the damper and, accordingly, over both pairing contact surfaces of the blade platform. For a seal wire damper (Fig. 2(b)), which has a circular cross section, contact is expected to be along lines and, hence, line friction contact elements are distributed over contact interfaces. For a strip damper (Fig. 2(c)), area contact elements are applied over one contact surfaces and line contact elements are distributed over an edge of the damper.

The friction interface elements allow calculation of the multiharmonic components of the contact interaction forces, $\mathbf{f}_e^{\text{loc}}(\mathbf{u}_e^{\text{loc}}) = \{\mathbf{f}_\tau, \mathbf{f}_\nu, \mathbf{f}_\zeta\}^T$, at each e th node of the FE mesh for a given multiharmonic component of relative displacements, $\mathbf{u}_e^{\text{loc}} = \{\mathbf{u}_x, \mathbf{u}_y, \mathbf{u}_z\}^T$, and they also allow calculation of a stiffness matrix of the contact

interface: $\mathbf{k}_e^{\text{loc}}(\mathbf{u}_e^{\text{loc}}) = \partial \mathbf{f}_e^{\text{loc}}(\mathbf{u}_e^{\text{loc}}) / \partial \mathbf{u}_e^{\text{loc}}$.

Due to the different nature of the contact forces acting in the plane of the contact and along a normal direction, the contact forces have to be calculated in a local coordinate system, τ, ν, ζ , with the ζ axis directed along the normal to the contact surface and the two other axes of this local Cartesian system, τ and ν , are located in a plane tangent to this contact surface. Each coordinate component of multiharmonic contact force and displacement here is a vector comprising $2n$ harmonic coefficients of an expansion of the forces and displacement, i.e.,

$$\mathbf{f}_\gamma = \{\tilde{f}_1^\gamma, \tilde{f}_1^\gamma, \dots, \tilde{f}_n^\gamma, \tilde{f}_n^\gamma\}^T, \quad \mathbf{u}_\gamma = \{\tilde{u}_1^\gamma, \tilde{u}_1^\gamma, \dots, \tilde{u}_n^\gamma, \tilde{u}_n^\gamma\}^T \quad (7)$$

where $\gamma = \tau, \nu, \zeta$ and n is the number of harmonics used in the multiharmonic representation of displacements.

Both the contact interaction forces and the contact stiffness matrix are generally strongly nonlinear and are dependent on the relative displacements. The analytical derivation of the expressions for $\mathbf{f}_e^{\text{loc}}(\mathbf{u}_e^{\text{loc}})$ and $\mathbf{k}_e^{\text{loc}}(\mathbf{u}_e^{\text{loc}})$ in Ref. [19] allows their exact and extremely fast calculation. In order to simulate the effects of three-dimensional friction contact interactions, two friction contact elements developed in Ref. [19] are applied in parallel for each contact node with directions of tangential motion for each of these two elements selected to be mutually perpendicular.

Relative displacements in the local coordinates are determined from vectors of displacements of blades, $\mathbf{u}_e^B = \{\mathbf{u}_x^B, \mathbf{u}_y^B, \mathbf{u}_z^B\}^T$, and dampers, $\mathbf{u}_e^D = \{\mathbf{u}_x^D, \mathbf{u}_y^D, \mathbf{u}_z^D\}^T$, at pairing nodes of the contact interface:

$$\mathbf{u}_e^{\text{loc}} = \mathbf{R}_e(\mathbf{u}_e^B - \mathbf{u}_e^D) \quad (8)$$

where $\mathbf{R}_e(6n \times 6n)$ is a matrix of transformation for the e th contact node from the global coordinate system to the local one.

In order to use the contact forces and stiffness matrices in the calculation of the whole bladed-disk-UPD system, they are transformed into the global coordinate system, which is used for the construction of the FE model for the bladed disk:

$$\mathbf{f}_e = \mathbf{R}_e^T \mathbf{f}_e^{\text{loc}}, \quad \mathbf{k}_e = \mathbf{R}_e^T \mathbf{k}_e^{\text{loc}} \mathbf{R}_e \quad (9)$$

Multiharmonic Balance Equation of Motion. In the method developed, a bladed disk and dampers are considered as elastic bodies, which are modeled separately by FE method, and then these models are condensed and combined in a coupled system using friction contact elements described in the preceding section.

The equation of motion for a coupled system bladed disk and dampers takes the following form:

$$\mathbf{K}\mathbf{q}(t) + \mathbf{C}\dot{\mathbf{q}}(t) + \mathbf{M}\ddot{\mathbf{q}}(t) + \mathbf{f}[\mathbf{q}(t)] - \mathbf{p}(t) = \mathbf{0} \quad (10)$$

where \mathbf{K} , \mathbf{C} , and \mathbf{M} are stiffness, damping, and mass matrices of the combined system, respectively, $\mathbf{f}[\mathbf{q}(t)]$ is a vector of nonlinear interface forces, and $\mathbf{p}(t)$ is a vector of excitation forces.

The steady-state periodic vibration response is calculated, and therefore, calculation can be efficiently done in the frequency domain using the multiharmonic balance method. In accordance with this method, displacements are represented by a restricted Fourier series:

$$\mathbf{q}(t) = \sum_{j=1}^n (\bar{\mathbf{q}}_j \cos m_j \omega t + \bar{\bar{\mathbf{q}}}_j \sin m_j \omega t) \quad (11)$$

where $\bar{\mathbf{q}}_j$ and $\bar{\bar{\mathbf{q}}}_j$ ($j=1, \dots, n$) are vectors of cosine and sine harmonic coefficients of the multiharmonic expansion (marked here and further by single and double bars above a symbol), and m_j ($j=1, \dots, n$) are specific numbers of harmonics that are kept in the displacement representation. Choice of the total number of harmonics n kept in the multiharmonic expansion and values selected for these harmonics m_j are determined by the solution accuracy required and by the calculated spectrum of the forced response: harmonics that can contribute significantly to the forced response

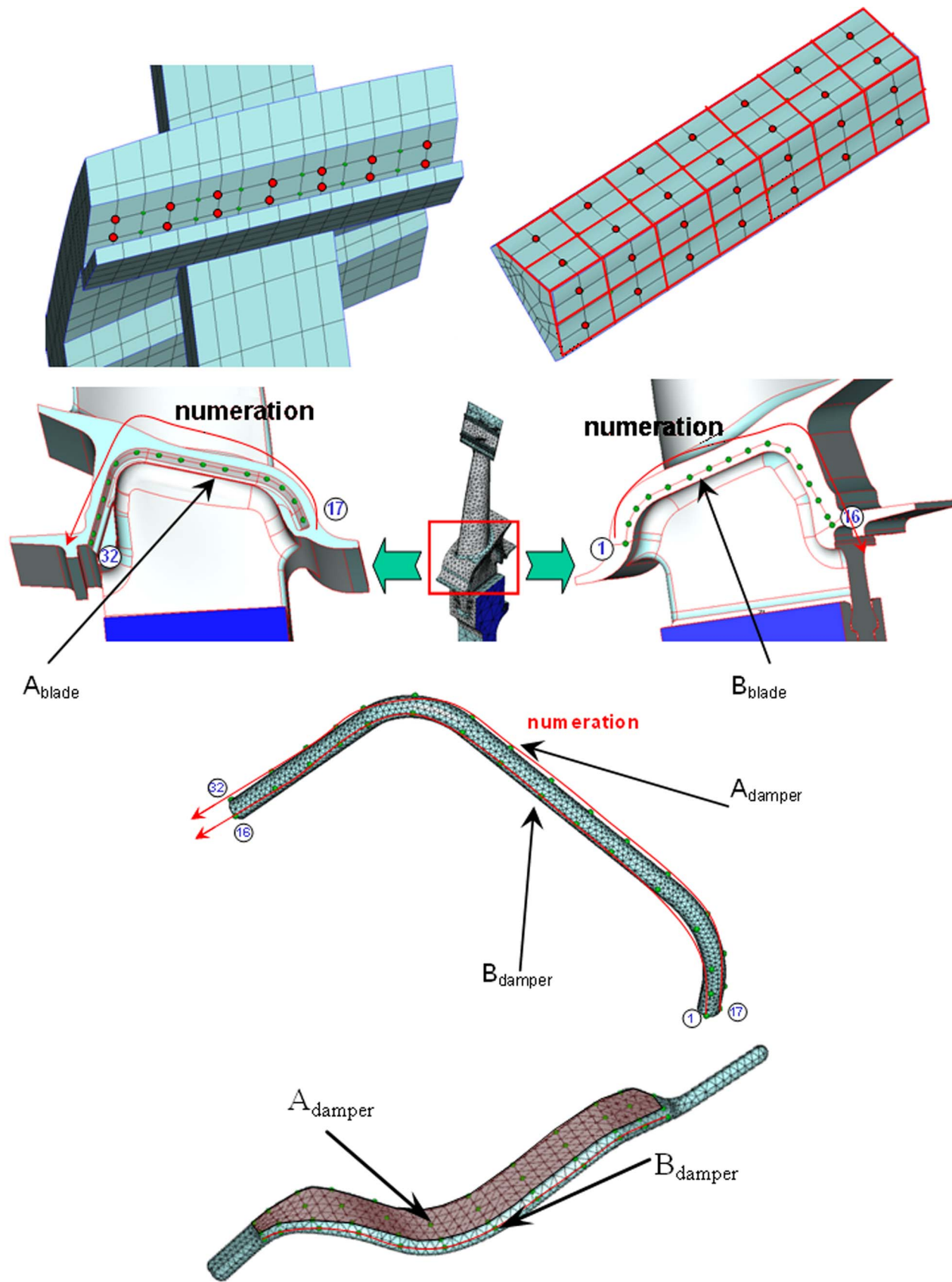


Fig. 2 Application of area and line friction contact interface elements: (a) a bladed disk with cottage-roof dampers, (b) a bladed disk with seal wires, and (c) a strip damper

should be included. For the search of major and superharmonic resonances, m_j is an integer number, and for the search of subharmonic and combination resonances, m_j can be a fractional number, appropriately selected. As a result, multiharmonic representation of the forced response allows the determination of periodic forced response even for strongly nonlinear structures including (i) major resonances, (ii) superharmonic resonances, (iii) subharmonic resonances, and (iv) combination resonances with any accuracy required.

Application of the multiharmonic balance method and use of the condensed matrix expressions of Eqs. (3)–(6) provide condensed equations of motion in the frequency domain. These equations are formulated exclusively for nonlinear DOFs, i.e., with respect to harmonic coefficients of the multiharmonic expansion for a set of DOFs located at contact interfaces. These equations take the form

$$\mathbf{R}_j = \begin{Bmatrix} \mathbf{Q}_j^B \\ \mathbf{Q}_j^D \end{Bmatrix} - \begin{Bmatrix} \text{lin} \mathbf{Q}_j^B \\ \text{lin} \mathbf{Q}_j^D \end{Bmatrix} + \begin{bmatrix} \mathbf{A}_j^B & \mathbf{0} \\ \mathbf{0} & \mathbf{A}_j^D \end{bmatrix} \begin{Bmatrix} \mathbf{F}_j(\mathbf{Q}^B, \mathbf{Q}^D) \\ -\mathbf{F}_j(\mathbf{Q}^B, \mathbf{Q}^D) \end{Bmatrix} = \mathbf{0} \quad (12)$$

where $j = \overline{1, n}$, and $\mathbf{Q}_j^B = \bar{\mathbf{Q}}_j^B + i\bar{\mathbf{Q}}_j^B$ and $\mathbf{Q}_j^D = \bar{\mathbf{Q}}_j^D + i\bar{\mathbf{Q}}_j^D$ are sought for vectors of complex amplitudes for the bladed disk and the damper, respectively, for the j th harmonic. Subscript j is added to $\text{lin} \mathbf{Q}_j^{B,D}$ and $\mathbf{A}_j^{B,D}$ to indicate that these vectors and matrices are evaluated for frequency $m_j\omega$ and m_j numbers of traveling waves. $\mathbf{F}_j(\mathbf{Q}^B, \mathbf{Q}^D)$ is a vector of complex amplitudes of the j th harmonic of the interaction forces acting at the contact interface. This vector is dependent on vectors $\mathbf{Q}^B = \{\mathbf{Q}_1^B, \mathbf{Q}_2^B, \dots, \mathbf{Q}_n^B\}^T$ and $\mathbf{Q}^D = \{\mathbf{Q}_1^D, \mathbf{Q}_2^D, \dots, \mathbf{Q}_n^D\}^T$, which include amplitudes of all harmonics for the bladed disk and the damper, and, therefore, the equations of motion given by Eq. (12) for all harmonics are coupled.

Calculation of the Multiharmonic Amplitudes. Equation (12) represents a nonlinear set of equations with respect to vector of multiharmonic amplitudes $\mathbf{Q} = \{\mathbf{Q}^B, \mathbf{Q}^D\}^T$. The Newton–Raphson method together with schemes of solution continuation/tracing is applied to solve this equation. An iterative Newton–Raphson solution process is expressed by the following formula:

$$\mathbf{Q}^{(k+1)} = \mathbf{Q}^{(k)} - \mathbf{J}^{-1}(\mathbf{Q}^{(k)})\mathbf{R}(\mathbf{Q}^{(k)}) \quad (13)$$

where superscript (k) indicates the number of the iteration and the real residuals vector $\mathbf{R}(\mathbf{Q})$ is formed from residual vectors obtained for each harmonic in Eq. (12):

$$\mathbf{R}(\mathbf{Q}) = \{\text{Re}(\mathbf{R}_1), \text{Im}(\mathbf{R}_1), \dots, \text{Re}(\mathbf{R}_n), \text{Im}(\mathbf{R}_n)\}^T \quad (14)$$

The iterative solution is terminated when a required accuracy is achieved, i.e., $\|\mathbf{R}(\mathbf{Q})\| < \varepsilon$. A Jacobian of Eq. (12) is determined as

$$\mathbf{J}(\mathbf{Q}) = \partial \mathbf{R}(\mathbf{Q}) / \partial \mathbf{Q} = \mathbf{I} + \mathbf{A}(\omega)\mathbf{K}_{\text{nl}}(\mathbf{Q}) \quad (15)$$

where \mathbf{I} is an identity matrix, $\mathbf{A}(\omega)$ is a real matrix formed from real and imaginary parts of the FRF matrices, and $\mathbf{K}_{\text{nl}}(\mathbf{Q}) = \partial \mathbf{F}(\mathbf{Q}) / \partial \mathbf{Q}$ is a stiffness matrix of the friction interface.

For the solution of Eq. (12) using the scheme given by Eq. (13), the nonlinear friction contact forces acting at blade-damper interfaces, $\mathbf{F}(\mathbf{Q})$, and the stiffness matrix of the friction contact interface, $\mathbf{K}_{\text{nl}}(\mathbf{Q})$, have to be calculated. These are formed by summing up vectors of nonlinear forces and stiffness matrices at all friction contact interfaces, i.e.,

$$\mathbf{F}(\mathbf{Q}) = \bigcup_{e=1}^{N_e} \mathbf{f}_e(\mathbf{Q}), \quad \mathbf{K}_{\text{nl}}(\mathbf{Q}) = \bigcup_{e=1}^{N_e} \mathbf{k}_e(\mathbf{Q}) \quad (16)$$

where N_e is the total number of contact elements. Since an analytical formulation is derived for the friction contact elements, these matrices are calculated very fast and exactly.

Test Case Studies

The methodology developed has been applied for the analysis of three different bladed disks with UPDs (see Fig. 2) of different types.

ADTurbII Blisk With Cottage-Roof Dampers. Forced response of a tuned ADTurbII blisk (see Refs. [11,21]) with cottage-roof UPDs is analyzed using explicit FE modeling of the damper. The blisk consists of 24 blades, and the FE model of one sector of the blisk used in the calculation contains 21,555 DOFs and the FE model of the cottage-roof damper contains 6146 DOFs.

For generation of the FRF matrices of the blisk, the first 32 natural frequencies and mass-normalized mode shapes were determined for each nodal diameter (cyclic index) involved in the forced response calculation. For generation of the FRF matrices of the cottage-roof damper, the first 24 natural frequencies and mass-normalized mode shapes were used.

The natural frequencies–nodal diameters diagram for this bladed disk is given in paper Ref. [18]. The background damping due to damping in the blisk material is assumed to be low: $\eta = 7.5 \times 10^{-5}$. Dissipation of vibration energy due to the friction forces produced by UPDs is calculated together with the forced response calculation. A 19th engine order traveling wave excitation pattern is studied.

Blade-damper interaction was modeled by 28 area friction contact elements distributed evenly on both sides of the cottage-roof damper. Area contact elements and nodes, which are used for determination of the contact stresses at the UPD, are shown in Fig. 2(a). Forced response level was determined at the blade tip.

Choice of Number of Harmonics Kept in a Solution. At the beginning of the numerical studies, the total number of harmonics required to be included in the multiharmonic forced response has to be determined.

To do this, the forced response was calculated with different numbers of harmonics kept in the multiharmonic expansion of the displacements, namely, 1, 2, and 3. In the multiharmonic expansion, first odd harmonics were used, namely, 19, 57, and 95 (which are the first, third, and fifth harmonics corresponding to the case of 19EO excitation analyzed). In order to be sure that the choice of number of harmonics will provide accurate results for the range of damper parameters to be explored, two cases were checked: (i) a case of nominal damper mass, 100%, and (ii) a heavy damper with mass value 1600% of its nominal value. The maximum displacements found over the vibration period and the amplitudes of each harmonic component included in the analysis are shown in Figs. 3(a) and 3(b), respectively. One can see that use of two first odd harmonics gives the forced response level practically identical to the case when three harmonics are included. Therefore, in further calculations, only two harmonics, 19th and 57th, are kept.

Effects of Damper Parameters on Forced Response. Results of the forced response calculation, obtained for different levels of static normal stresses, are shown in Fig. 4. This variation of static normal stresses can be achieved in practice by a change in the damper mass. Cases of the normal stresses corresponding to a damper mass from 50% of the nominal value to 12,800% were studied. One can see that for lower damper mass values (from 50% to 100%), the resonance frequency for the blisk with dampers is close to the resonance frequency of the 1F mode of the blisk without dampers. For higher mass values (from 6400% to 12,800%), this resonance frequency is close to the resonance frequency of the blisk with fully stuck dampers. For mass values from 200% to 1600%, the resonance frequency of the blisk with dampers takes intermediate values between resonance frequencies of linear systems: (i) the blisk without dampers and (ii) the blisk with stuck dampers. For low values of the static normal stresses (i.e., 50% and 100%), separation of contact surfaces has been observed over a large part of the contact interface area, which

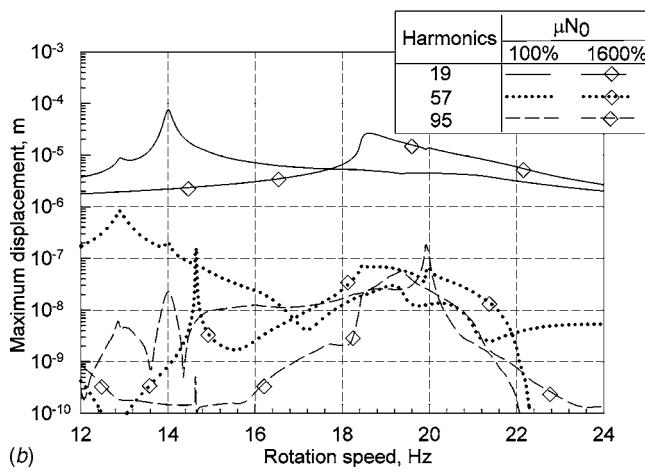
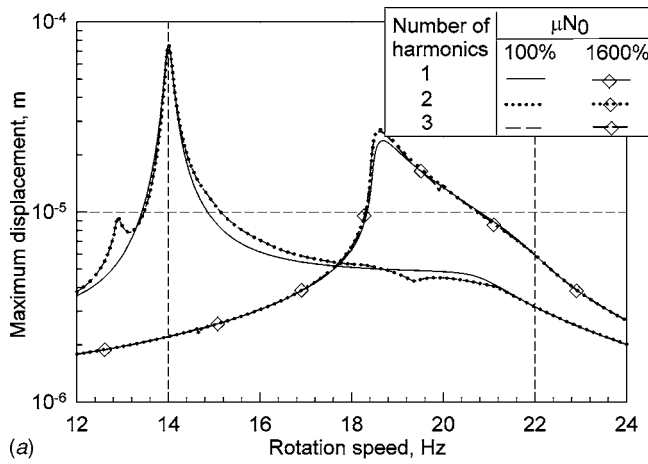


Fig. 3 Forced response levels calculated with different numbers of harmonics: (a) maximum displacement and (b) amplitudes of harmonic components

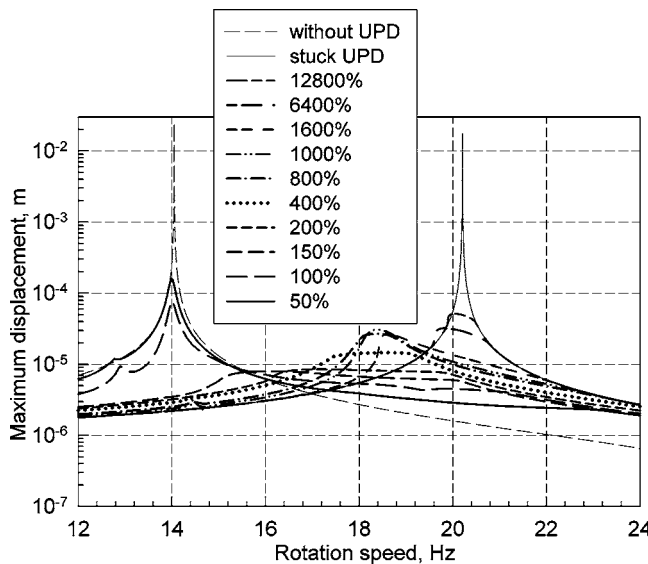


Fig. 4 Forced response of the blisk: effects of levels of the normal contact stresses/damper mass

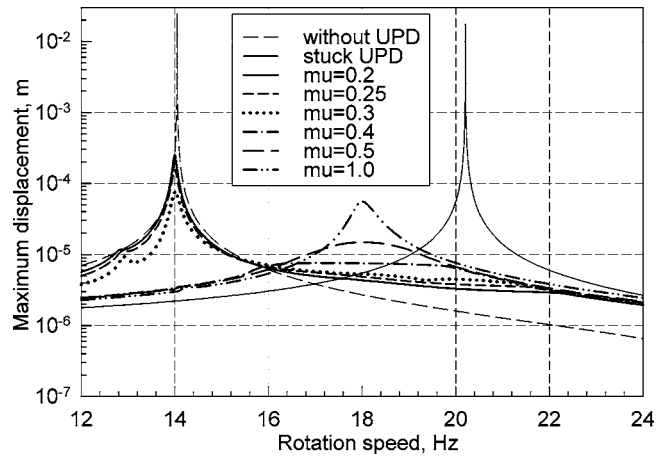


Fig. 5 Forced response of the blisk: effect of friction coefficient value

indicates possibility of the so-called damper clapping.

Forced response levels calculated for the nominal 100% damper mass value, but with different friction coefficients, are shown in Fig. 5.

Dependency of resonance frequency and resonance amplitude on parameters of the contact interfaces, such as (i) friction coefficient value and (ii) normal load level, is plotted in Fig. 6. One can see that the resonance frequency for friction coefficient values less than 0.3 is close to the resonance frequency of the blisk without dampers (resonance rotation speed of 14 Hz). When the friction coefficient varies from 0.3 to 0.5, the resonance frequency changes significantly; for higher friction coefficient values from 0.5 to 1.0, the resonance frequency is almost constant (resonance rotation speed of 18 Hz). Both the normal load and the friction coefficient significantly affect the resonance response level, which can be reduced for this blisk by factor of 10^3 by appropriate choice of friction coefficient or normal load.

Bladed Disk With Seal Wire Dampers. Another structure analyzed is a high pressure turbine bladed disk which comprises 114 blades with seal wire dampers (see Fig. 1(b)) fitted in special cavities underneath the blade platform. The seal wires are in contact with adjacent blades and they dissipate vibration energy similar to conventional cottage-roof UPDs. FE models contain (i) 314,187 DOFs for a single bladed disk sector and (ii) 37,785

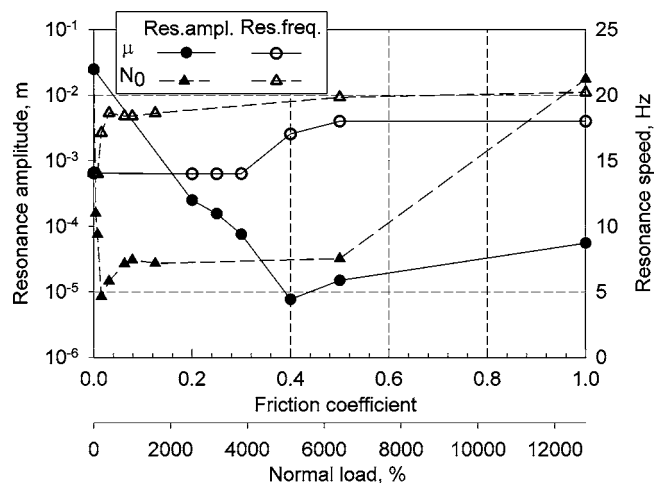


Fig. 6 Dependency of the resonance rotation speed and amplitude on contact parameters: (i) friction coefficient and (ii) normal load

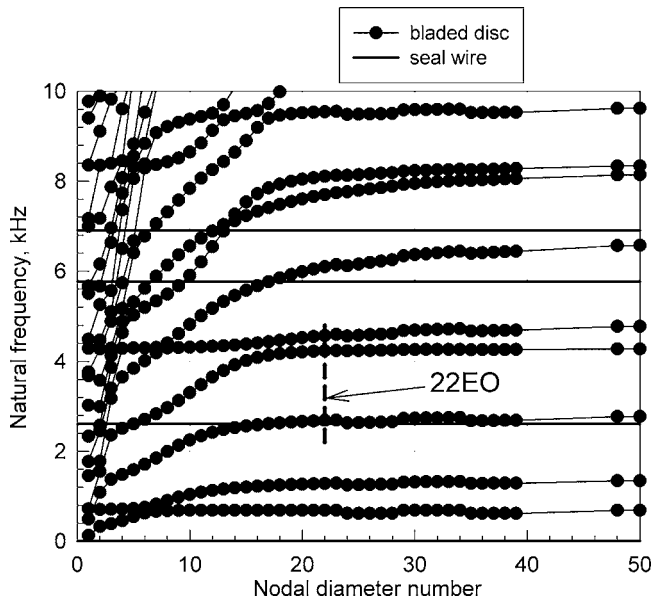


Fig. 7 Motion of the cottage-roof damper and blade platforms over vibration period

DOFs for a seal wire damper. Excitation by 22EO excitation was considered, and the damping loss factor, which is due to material energy dissipation, is assumed to be 0.005.

For generation of the FRF matrices for the blisk, the first 48 natural frequencies and mass-normalized mode shapes were determined for each nodal diameter involved in the forced response calculation. For generation of the FRF matrices of the seal wire, the first 48 natural frequencies and mass-normalized mode shapes were calculated. The lower natural frequencies of the bladed disc and of the damper are plotted in Fig. 7. In this figure, the frequency range analyzed is also shown. Due to its high flexibility, the seal wire natural frequencies are close to the natural frequencies of the bladed disk. In the frequency range of interest, there are natural frequencies of the bladed disk and of the seal wire and, hence, the seal wire deforms significantly when vibrating in this frequency range. Therefore, the seal wire cannot be modeled as a rigid body, and allowing for its dynamic properties is essential for accurate forced response analysis.

The number of harmonics necessary for accurate forced response calculation was decided by comparison of the forced re-

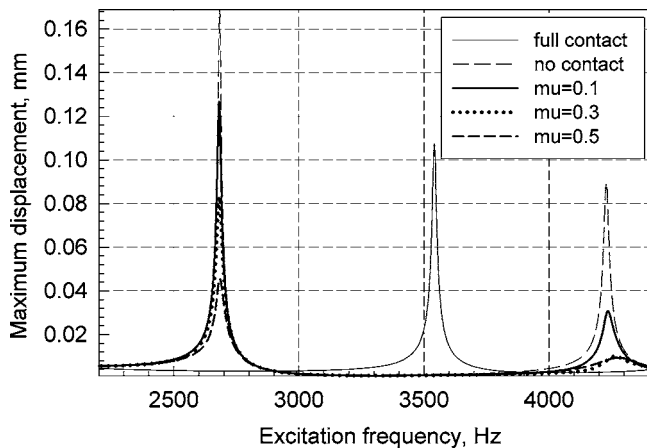


Fig. 8 Forced responses under 100% excitation and normal load levels

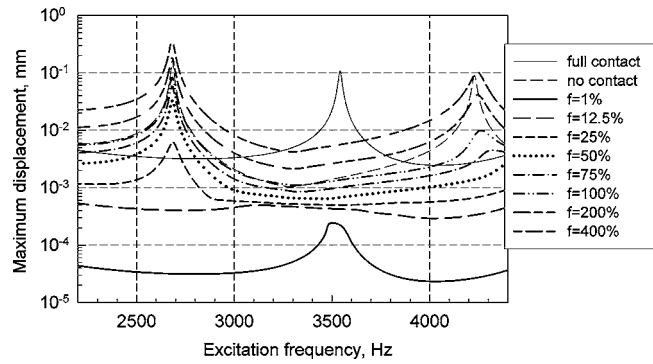


Fig. 9 Forced response levels for different excitation levels ($\mu=0.3$ and 100% normal load level)

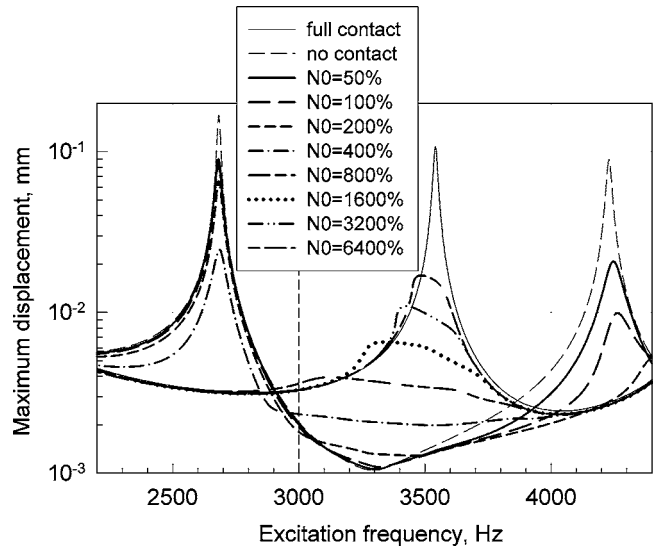


Fig. 10 Forced response for different normal loads applied at contact nodes ($\mu=0.3$ and 100% excitation level)

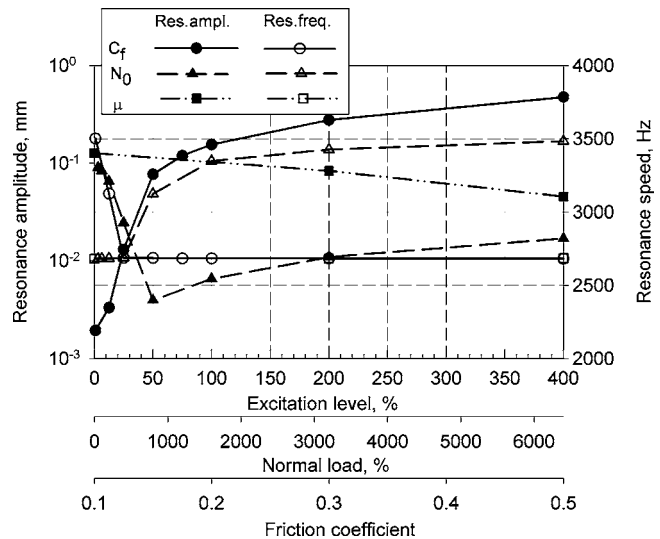


Fig. 11 Dependency of the resonance rotation speed and amplitude on (i) excitation level, (ii) normal load, and (iii) friction coefficient

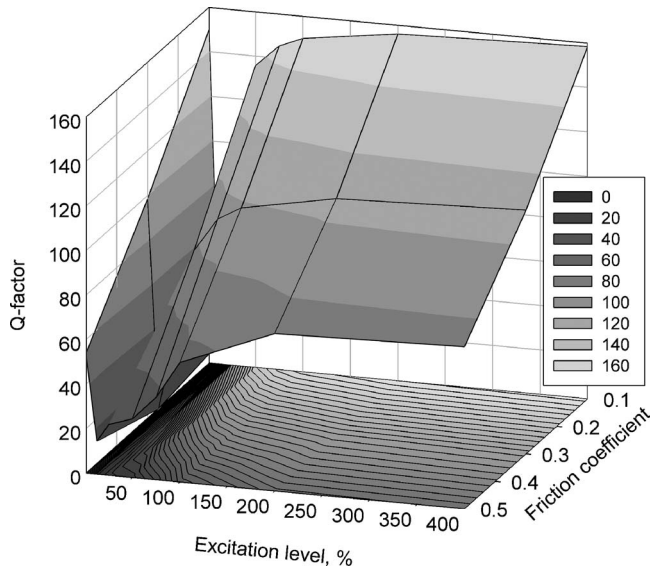


Fig. 12 Dependency of the Q factor on the excitation level and friction coefficient (a case of $N_0=100\%$)

sponses obtained with one, two, and three first odd harmonics of the 22EO excitation. Since for all three cases considered the results are very close, in further analysis, only one harmonic was used.

Effects of the friction coefficient values, excitation levels, and normal load levels on the forced response characteristics are shown in Figs. 8–10. In all these figures, forced responses of the bladed disk for two limiting cases are also plotted for comparison: (i) a forced response of the bladed disk without dampers (a solid

black line) and (ii) a forced response of the bladed disk with fully stuck dampers (a dashed black line). 100% excitation level was considered for both these limiting cases.

Figure 8 demonstrates significant influence of the friction coefficient on resonance forced response. Noticeable variation of the resonance frequencies can also be observed. From Fig. 9, one can see that the damping effect of the seal wire is evident for all excitation force levels. Even for an excitation level of 1% of its nominal value, the forced response of a structure with dampers is significantly lower than that for the case when dampers are absent or when they are fully stuck. For a 1% excitation level, the first resonance frequency of the bladed disk with dampers is close to the first resonance frequency of a bladed disk with fully stuck dampers. For the other excitation levels considered here, the first resonance frequency is close to the resonance frequency of a bladed disk without dampers.

Results displayed in Fig. 10 show that only for extremely high levels of normal loads at contact interfaces (from 1600% to 6400%) does the resonance frequency approach the resonance frequency of the bladed disk with fully stuck dampers. For all realistic values, from 50% to 800%, they are close to the resonance frequency of the bladed disk without dampers.

Resonance frequency and amplitude are plotted in Fig. 11 as functions of friction coefficient, excitation level, and level of normal load. The results show high sensitivity of the resonance response levels to damper parameters: a small variation of any of the parameters considered can change forced response level by several times and the resonance frequency can be changed by up to 40% in some ranges of parameter variation. However, the resonance frequency appears to be insensitive, for the considered case, to variation of friction coefficient from 0.1 to 0.5.

The Q factor was extracted from the forced response calculations, and its dependency on the friction coefficient and the excitation level is shown in Fig. 12 in the form of 3D mesh and contour plots.

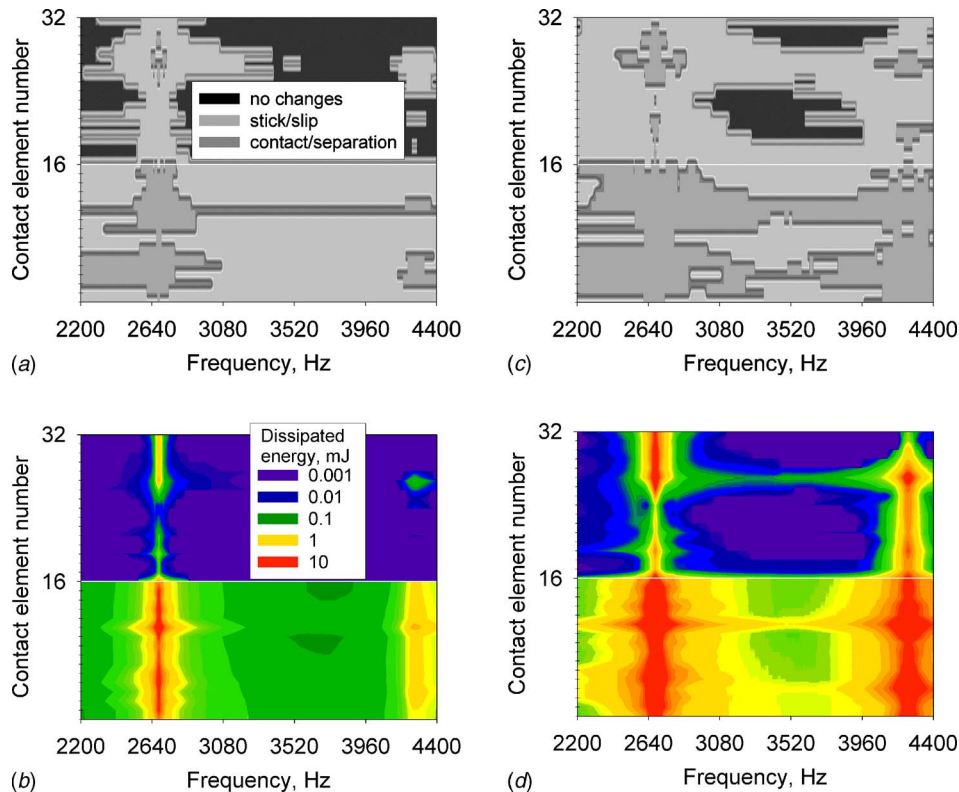


Fig. 13 Contact conditions and energy dissipated (mJ) by each of the 32 friction contact elements for two excitation levels: (a) 100% and (b) 400%

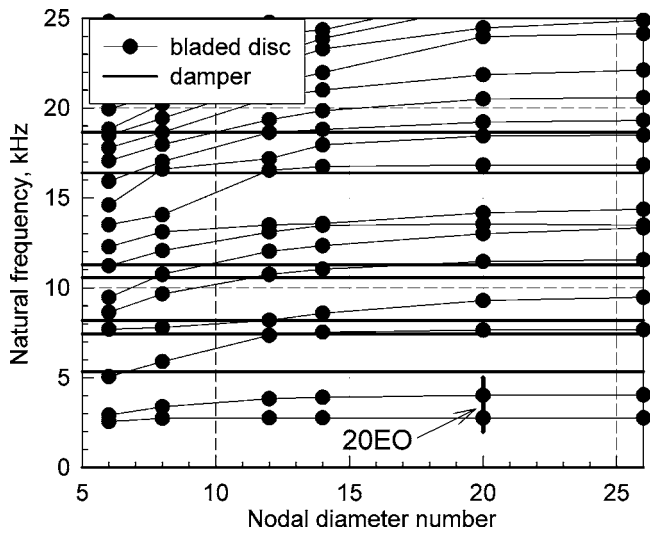


Fig. 14 Natural frequencies of the bladed disc and of the UPD

The friction contact interface elements allow the determination, for each element, of the (i) contact conditions and (ii) energy dissipated over the area covered by this element.

The contact conditions are determined over the period of vibration for each excitation frequency, and the following conditions are indicated for each contact interface element:

- (i) no change in contact conditions, i.e., the pairing nodes at both sides of a contact interface are in contact and remain stuck over the vibration period or the pairing nodes are separated and remain separated over the whole vibration period
- (ii) stick-slip transition, i.e., the pairing nodes are always in contact and a slip-stick transition occurs at least once during the vibration period
- (iii) contact-separation transition, i.e., contact-to-separation or separation-to-contact transition of the contact state occurs at least once over the vibration period. Slip-stick transitions can also occur during intervals when nodes are in contact.

Energy dissipated over a vibration period is also calculated for each friction contact element. Plots indicating contact condition and energy dissipated by each of the 32 friction contact elements

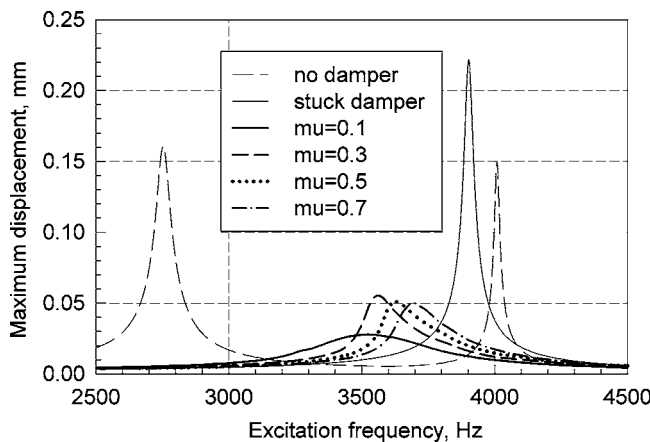


Fig. 15 Forced responses for different friction coefficient values

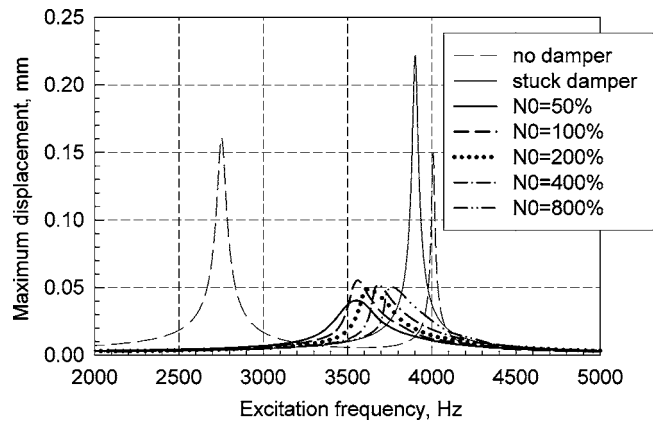


Fig. 16 Forced response levels for different normal loads at contact interfaces

over the whole frequency range analyzed are shown in Fig. 13.

Three possible contact conditions are indicated by different colors: (i) a case without contact condition changes is colored blue, (ii) a case of slip-stick transitions without contact separation is green, and (iii) a case of contact-separation transition is red. Contour lines of the dissipated energy are plotted in a logarithmic scale. The legend explaining the color scheme used for indication of energy dissipation levels is also given in Fig. 13. One can see that, for a case of 100% excitation level, majority of contact nodes are slipping or separating, although at contact interface A (see Fig. 2(b)), there is still a large area that is fully stuck over a wide excitation frequency range. Increase of the excitation level to 400% increases the number of contact elements where contact separation occurs. In all cases, most energy is dissipated at contact interface B.

Bladed Disk With Strip Dampers. The third bladed disk analyzed has 54 blades. A novel damper design was applied in this assembly: seal damper strips. The FE model of this damper is shown in Fig. 1(c). A FE model of a bladed disk sector used in the analysis contains 309,990 DOFs, and a FE model of the damper strip contains 24,753 DOFs. 45 friction contact elements were distributed over two contact interfaces of the damper and, accordingly, over pairing surfaces of the blade platforms: 32 area contact elements distributed over a contact surface marked by letter A in Fig. 1(c) and 13 line contact elements at an interface marked by letter B.

For generation of the FRF matrices of the bladed disk, the first

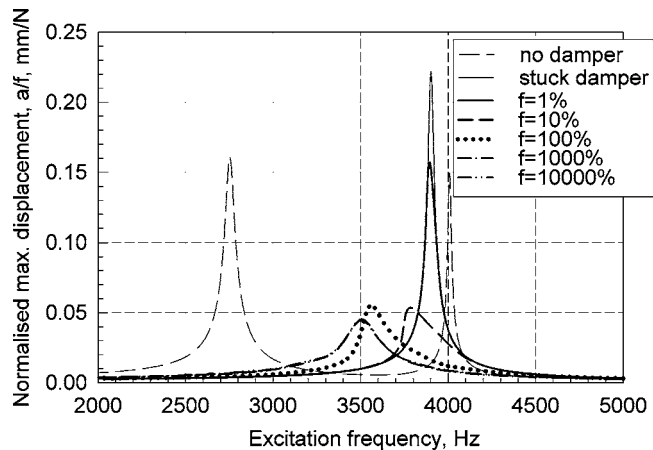


Fig. 17 Normalized forced response under different excitation levels

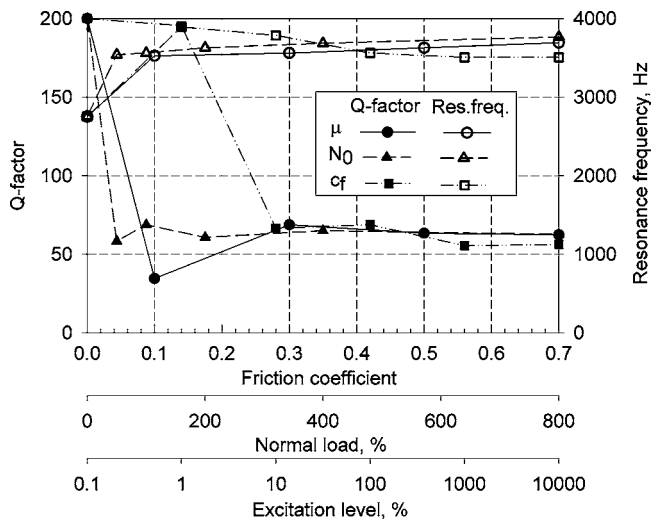


Fig. 18 Dependency of the resonance frequency and Q factor on (i) excitation level, (ii) normal load, and (iii) friction coefficient value

48 natural frequencies and mass-normalized mode shapes were determined for each nodal diameter involved in the forced response calculation. For generation of the FRF matrices of the damper strip, the first 48 natural frequencies and mass-normalized mode shapes were used. Excitation by 20EO is considered and the inherent damping loss factor, assumed for a case when dampers

are not fitted, is 0.005.

The lower natural frequencies of the bladed disk and of the damper strip are plotted in Fig. 14. One can see that the strip damper has natural frequencies that are close to the natural frequencies of the bladed disk, and they are located within frequency ranges analyzed; allowance for flexibility of the damper is therefore essential for accurate calculations.

Analysis of the number of harmonics necessary showed that use of only one harmonic can incur 30% error in the determination of forced response levels. The results obtained with 3 and higher number of harmonics, and therefore, two first odd harmonics of 20EO were used in the calculations: 20th and 60th.

Forced response levels calculated for different friction coefficient values are shown in Fig. 15.

For comparison, forced responses of two limiting linear structures are also plotted in this figure: (i) forced response of the bladed disk without dampers and (ii) forced response of the bladed disk with fully stuck dampers. One can see that the friction coefficient value significantly affects the resonance level and the resonance frequency. The resonance frequency of the bladed disks with strip dampers is located between resonance frequencies of the limiting linear cases. For higher friction coefficient values, it is closer to the resonance frequency of the bladed disk with fully stuck dampers; for $\mu=0.1$, the resonance frequency is almost centered between resonance frequencies of the bladed disk without and with stuck dampers. The lowest level of resonant forced response is achieved for $\mu=0.1$.

Forced response levels calculated for different static normal stresses are shown in Fig. 16.

Normalized forced response levels calculated for different ex-

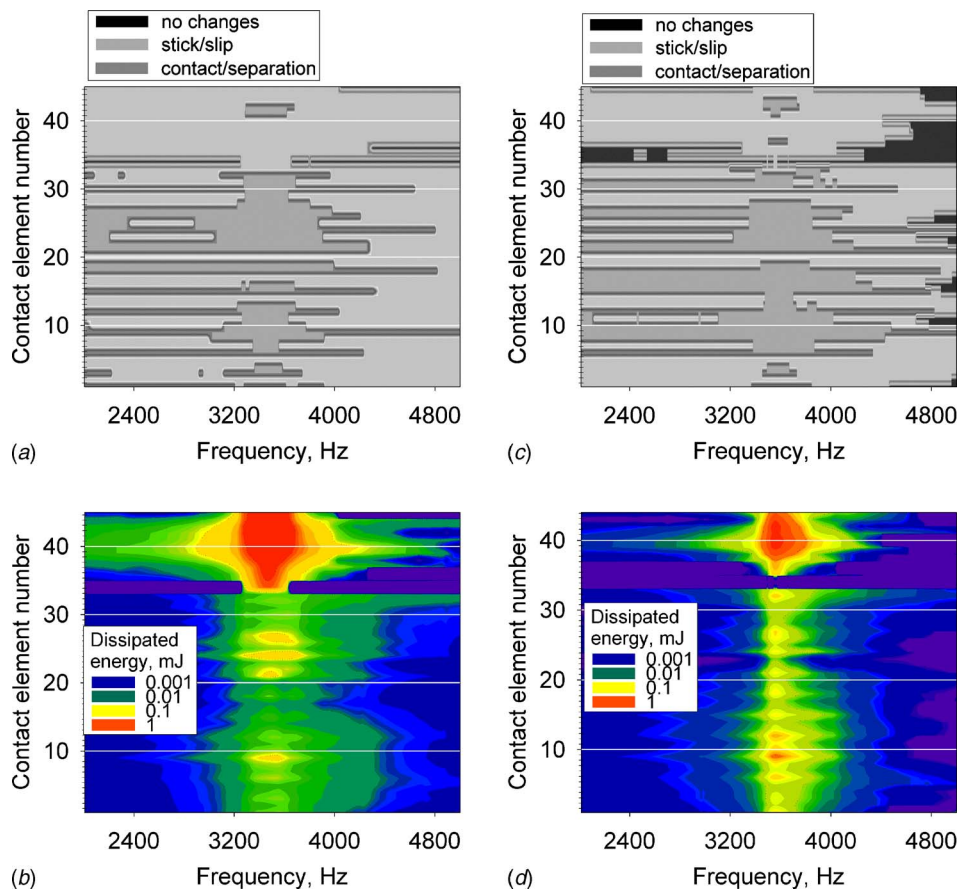


Fig. 19 Contact conditions for each of the 45 friction contact elements: (a) $\mu=0.1$ and (b) $\mu=0.3$

citation levels are shown in Fig. 17. The normalization is performed by dividing the forced response by the excitation level coefficient. This normalization allows comparison of nonlinear effects of dampers on forced response: for the case of linear vibrations, all curves would be identical. One can see that for excitation levels varying from 1% to 1000%, normalized amplitude levels and resonance frequencies are different. However, for high excitation levels, from 1000% to 10,000%, normalized forced response curves are almost identical, which indicates smaller nonlinear effects for high level of excitation.

Effects of all parameters analyzed on the resonance frequency and Q factor are summarized in Fig. 18. It is important to notice the high robustness of the damping properties of this damper design: for wide ranges of variation of damper parameters and excitation levels the damper exhibits stable, almost constant values for the resonance frequency and damping characteristics.

Examples of contact condition and energy dissipation plots for each of the 45 friction contact elements, over the whole frequency range analyzed, are shown in Fig. 19.

One can see that the number of contact nodes that experienced temporary separation is larger for higher values of the friction coefficient. In all cases analyzed, the dominant part of the vibration energy is dissipated at the contact interface marked by letter B in Fig. 1(c).

Conclusions

A generic method for the analysis of nonlinear forced response for bladed disks with friction damping devices of different designs has been developed. The method allows the use of explicit FE models of dampers, which can accurately describe any complex geometric shape, flexibility, and, for the first time, dynamic properties of dampers in multiharmonic analysis of bladed disks.

Steady-state, strongly nonlinear forced response is calculated by a multiharmonic balance method in conjunction with an original analytical formulation for the extended Jacobian of the nonlinear equations and for evaluation of nonlinear contact forces and contact stiffnesses.

Large-scale FE damper and bladed disk models containing 10^4 – 10^6 DOFs can be used in order to describe the complex geometric shape of modern dampers and bladed disks of different designs with any required level of refinement.

Detailed description of contact interactions over area and line contact interfaces between damper and blades is achieved by especially developed friction contact elements. These elements allow for friction, stick slip, and contact-separation contact state transitions. Effects of normal load variation not only on tangential friction force level but also on time instant of stick slip are included in the friction modeling.

Numerical studies of realistic bladed disks with three different types of UPDs have been performed: (i) a cottage-roof damper, (ii) a seal wire damper, and (iii) a strip damper. Effects of contact interface parameters and excitation levels on damping properties of the dampers on forced response have been extensively explored.

For the first time, dampers of highly flexible design, such as seal wire dampers and strip damper, have been studied, and, moreover, distributions over contact interface areas for energy dissipated and for contact conditions have been calculated.

Acknowledgment

The author is grateful to Rolls-Royce plc. for providing the financial support for this project and for giving permission to publish this work.

References

- [1] Sanliturk, K. Y., Ewins, D. J., and Stanbridge, A. B., 2001, "Underplatform Dampers for Turbine Blades: Theoretical Modelling, Analysis and Comparison With Experimental Data," *Trans. ASME: J. Eng. Gas Turbines Power*, **123**, pp. 919–929.
- [2] Csaba, G., 1998, "Forced Response Analysis in Time and Frequency Domains of a Tuned Bladed Disk With Friction Dampers," *J. Sound Vib.*, **214**(3), pp. 395–412.
- [3] Jareland, M. H., 2001, "A Parametric Study of a Cottage Roof Damper and Comparison With Experimental Results," ASME Paper No. 2001-GT-0275.
- [4] Yang, B.-D., and Menq, C.-H., 1998, "Characterization of Contact Kinematics and Application to Design of Wedge Dampers in Turbomachinery Blading," *Trans. ASME: J. Eng. Gas Turbines Power*, **119**, pp. 410–423.
- [5] Zucca, S., Borrajo, J., and Gola, M. M., 2006, "Forced Response of Bladed Disks in Cyclic Symmetry With Underplatform Dampers," ASME Paper No. GT2006-90785.
- [6] Szwedowicz, J., Kissel, M., Ravindra, B., and Kellerer, R., 2001, "Estimation of Contact Stiffness and Its Role in the Design of a Friction Damper," ASME Paper No. GT-2001-0290.
- [7] Koh, K. H., Griffin, J. H., Filippi, S., and Akay, A., 2005, "Characterization of Turbine Blade Friction Dampers," *ASME J. Eng. Gas Turbines Power*, **127**(4), pp. 856–862.
- [8] Koh, K.-H., and Griffin, J. H., 2006, "Dynamic Behaviour of Spherical Friction Dampers and Its Implication to Damper Contact Stiffness," *Proceedings of ASME Turbo Expo*, Barcelona, Spain, May 8–11.
- [9] D'Ambrosio, F., Chatelet, E., and Jacquet, G., 2005, "Influence of Contact States on the Dynamic Behavior of Rubbing Structures," ASME Paper No. GT2005-68560.
- [10] Panning, L., Sextro, W., and Popp, K., 2003, "Spatial Dynamics of Tuned and Mistuned Bladed Disks With Cylindrical and Wedge-Shaped Friction Dampers," *Int. J. Rotating Mach.*, **9**(3), pp. 219–228.
- [11] Petrov, E. P., and Ewins, D. J., 2007, "Advanced Modelling of Underplatform Friction Dampers for Analysis of Bladed Disc Vibration," *ASME J. Turbomach.*, **129**, pp. 143–150.
- [12] Petrov, E. P., and Ewins, D. J., 2004, "State-of-the-Art Dynamic Analysis for Nonlinear Gas Turbine Structures," *Proc. IMechE: J. Aerosp. Eng.*, **218**(G3), pp. 199–211.
- [13] Yeo, S., and Kielb, J., 2002, "The Application of a Numerical Code to the Optimisation of Inter-Platform Damping Technology," *Proceedings of the Seventh HCF Conference*, FL, May 14–17.
- [14] Firrone, C. M., Botto, D., and Gola, M. M., 2002, "Modelling a Friction Damper: Analysis of the Experimental Data and Comparison With Numerical Results," *Proceedings of ESDA2006, Eighth Biennial ASME Conference on Engineering Systems Design and Analysis*, Torino, Italy, July 4–7.
- [15] Szwedowicz, J., Gibert, C., Sommer, T. P., and Kellerer, R., 2006, "Numerical and Experimental Damping Assessment of a Thin-Walled Friction Damper in the Rotating Set-Up With High Pressure Turbine Blades," ASME Paper No. GT2006-90951.
- [16] Petrov, E. P., 2003, "A Method for Use of Cyclic Symmetry Properties in Analysis of Nonlinear Multiharmonic Vibrations of Bladed Discs," ASME Paper No. GT-2003-38480.
- [17] Petrov, E. P., and Ewins, D. J., 2005, "Method for Analysis of Nonlinear Multiharmonic Vibrations of Mistuned Bladed Discs With Scatter of Contact Interface Characteristics," *ASME J. Turbomach.*, **127**, pp. 128–136.
- [18] Petrov, E. P., and Ewins, D. J., 2005, "Mistuning Effects on Forced Response of Bladed Discs With Friction Dampers," *Proceedings of NATO Symposium: Evaluation, Control and Prevention of High Cycle Fatigue in Gas Turbine Engines for Land, Sea and Air Vehicles*, Granada, Spain, Oct. 3–5, Paper No. 38–1.
- [19] Petrov, E. P., and Ewins, D. J., 2003, "Analytical Formulation of Friction Interface Elements for Analysis of Nonlinear Multi-Harmonic Vibrations of Bladed Discs," *ASME J. Turbomach.*, **125**, pp. 364–371.
- [20] Petrov, E. P., and Ewins, D. J., 2006, "Effects of Damping and Varying Contact Area at Blade-Disc Joints in Forced Response Analysis of Bladed Disc Assemblies," *ASME J. Turbomach.*, **128**, pp. 403–410.
- [21] Elliott, R., Green, J. S., and Seinturier, E., 2005, "Aeroelastic Design of Turbine Blades-ADTurB II Overview," *Sixth European Turbomachinery Conference*, Lille, France, March 7–11, Paper No. AMP-105-01/62.